

Article

Sorption of Ag⁺ and Cu²⁺ by Vermiculite in a Fixed-Bed Column: Design, Process Optimization and Dynamics Investigations

Olga Długosz  and Marcin Banach * 

Faculty of Chemical Engineering and Technology, Institute of Chemistry and Inorganic Technology, Cracow University of Technology, Warszawska 24, 31-155 Cracow, Poland; odlugosz@chemia.pk.edu.pl

* Correspondence: marcinbanach@chemia.pk.edu.pl; Tel.: +48-12-628-2092

Received: 15 October 2018; Accepted: 9 November 2018; Published: 11 November 2018



Abstract: Vermiculite has been used for the removal of Cu²⁺ and Ag⁺ from aqueous solutions in a fixed-bed column system. The effects of initial silver and copper ion concentrations, flow rate, and bed height of the adsorbent in a fixed-bed column system were investigated. Statistical analysis confirmed that breakthrough curves depended on all three factors. The highest inlet metal cation concentration (5000 mg/dm³), the lowest bed height (3 cm) and the lowest flow rate (2 and 3 cm³/min for Ag⁺ and Cu²⁺, respectively) were optimal for the adsorption process. The maximum total percentage of metal ions removed was 60.4% and 68.7% for Ag⁺ and Cu²⁺, respectively. Adsorption data were fitted with four fixed-bed adsorption models, namely Clark, Bohart–Adams, Yoon–Nelson and Thomas models, to predict breakthrough curves and to determine the characteristic column parameters. The adsorbent was characterized by SEM, FTIR, EDS and BET techniques. The results showed that vermiculite could be applied as a cost-effective sorbent for the removal of Cu²⁺ and Ag⁺ from wastewater in a continuous process.

Keywords: fixed-bed column; sorption dynamics; silver; copper; vermiculite

1. Introduction

One of the greatest environmental problems today is the presence of harmful and hazardous substances in industrial wastewater. Pollution in the ecosystem significantly affects the quality of water, and thus the life of plants and animals [1]. Some of the worst pollutants are heavy metals, which are released into the environment through natural process and anthropogenic activities. Due to accumulation, even small concentrations can significantly worsen the condition of the environment [2]. The increasing contamination of these substances necessitates their removal from wastewater and post-process water [3]. Examples of such metals are copper and silver. In recent years, the above-mentioned metals have been widely used in utility products (cosmetics, cleaning agents and impregnated functional coatings, among others) as biocidal agents. The elements occur in products as nanoparticles as well as ions, which affects their concentration in wastewater [4]. Small-sized nanoparticles demonstrate increased reactivity, which simultaneously reduces a particle's lifetime in the environment. The reactivity of the particles may cause an increased degree of aggregation, changes in an oxidation state or a tendency to precipitate. Modifications of the structure of particles occurring in the environment strongly affect their surface properties and, consequently, transport and behaviour in water systems, soils, and their impact on organisms [5].

Conventional methods for removing heavy metals from aqueous solutions include filtration, chemical precipitation, coagulation and ion exchange [6,7]. These methods are not effective unless the concentration of a metal in the sewage is relatively high. Adsorption is one of the alternative

technologies for removing metal ions, which is an efficient method even for low metal ion concentrations. Recently, research has been focused on “green adsorption”. This method places particular emphasis on the natural origin of sorbents, lower acquisition costs and the possibility of using materials of waste origin, for example, from agricultural and food industries [8–10]. Examples of natural adsorbents are biosorbents, aluminosilicates, zeolites and fly ash [11]. Clay minerals are an increasingly important group of natural adsorbents [12,13]. The main advantage of using clay minerals are their relatively easy availability and natural origin, low production cost, and high thermal and mechanical resistance. An example of clay minerals is vermiculite, which is a hydrated mineral magnesium and iron silicate [14,15]. Vermiculite is a good adsorbent for removing ions from aqueous solutions because of an insufficient electron charge. Cations are exchanged at planar sites, resulting from the interactions between metal ions and the negative permanent charge (outer-sphere complexes) [16,17].

This work investigated the possibility of using vermiculite as an adsorbent of silver and copper ions. The adsorption process was carried out in a continuous system that evaluated the efficiency of the removal of copper and silver ions from aqueous solutions. The influence of process parameters and the effectiveness of the applied sorption method were studied. In addition, a mathematical description of the dynamics of the adsorption process analysis was presented.

2. Materials and Methods

2.1. Materials

Silver nitrate [AgNO₃] (POCH, Gliwice, Poland, 99.9% purity) and copper sulphate [CuSO₄·5H₂O] (Sigma Aldrich, Saint Louis, MO, USA, 98% purity) were used as sources of Ag⁺ and Cu²⁺ ions, respectively. Vermiculite [Al_{0.57}H_{1.4}Mg_{1.705}O_{7.86}Si_{1.43}] was purchased from a commercial supplier from Poland. All chemicals were used without any further purification. Solutions were prepared using analytical grade reagents and high purity deionized water.

Expanded vermiculite was used in the research. In the first step, vermiculite was chemically activated by leaching it with a 10% citric acid solution and a 0.1 M NaOH solution for the adsorption of copper and silver ions, respectively (1 g vermiculite per 10 cm³ base or acid solution). After one hour of stirring, solid residues were washed and dried at 105 °C for 24 h. The activation method was established in a previous study [18].

2.2. Methods

The surface morphology of vermiculite was determined using a scanning electron microscope (Vegall-Tescan Company, Brno-Kohoutovice, Czech Republic). The study was supplemented with micro area analysis using the EDS detector. The sorbent surface and pore sizes were determined by a low temperature sorption study performed by Micromeritics ASAP2010 (Norcross, GA, USA). Raw and modified vermiculite samples were subjected to FTIR analysis. Infrared spectra were obtained using an FTIR spectroscope (Nicolet 380, Thermo Scientific Brand, USA), where the spectra were recorded from 3900 to 400 cm⁻¹. The structure of the raw and activated materials was studied by analysis of XRD patterns. A Philips X’Pert camera (Malvern, UK) with monochromator PW 1752/00 CuKα was used in the study. In order to characterize the adsorption material, densimetric analyses were made using the pycnometric method. Bulk density and porosity were also established.

Actual density of a substance is the ratio of the material mass to its volume (the core of the material without pores):

$$d_a = \frac{m_m}{V_a} \quad (1)$$

Apparent density (pycnometric density) is the ratio of the sample weight to the total volume of the sample (the core of the material and open pores):

$$d_p = \frac{m_m}{V_p} \quad (2)$$

Bulk density is the ratio of weight to volume of a material without compaction:

$$d_b = \frac{m}{V} \quad (3)$$

Relative density is the ratio of bulk density to actual density:

$$d_r = \frac{d_b}{d_a} \times 100\% \quad (4)$$

Total porosity describes the number of pores per unit volume. It is calculated from the following equation:

$$P_t = \left(1 - \frac{d_b}{d_a}\right) \times 100\% \quad (5)$$

Open porosity of the analyzed material is determined from the equation:

$$P_o = \left(1 - \frac{d_b}{d_p}\right) \times 100\% \quad (6)$$

2.3. Continuous Column System

The adsorption of heavy metals on vermiculite was studied using the continuous column method. Adsorption measurements were carried out in a glass column with a diameter $D = 1.2$ cm and height $H = 12$ cm. The bed consisted of vermiculite with an average particle diameter of 0.866 mm. A solution of metal ions was fed at the top and the combination vacuum pump was connected at the bottom of the column. Liquid samples were collected at the bottom of the column at equal intervals. The concentration of metal ions in aqueous solutions was determined with silver sulphate, copper and reference electrodes (Hydromet Company, Gliwice, Poland) combined with the Elmetron CX-701 Multifunction Meter.

2.4. Statistical Analysis

The influence of sorption parameters of metal ions on vermiculite was determined by performing a series of continuous column measurements. Table 1 shows the input factors taken into account and the extent of their variation. The sorption capacity, calculated from Equation (8), was assumed as the output factor:

$$q_{eq} = \frac{Q \cdot A}{1000 \cdot m} = \frac{Q}{1000 \cdot m} \int_{t=0}^{t=t_{total}} C(t) dt \quad (7)$$

where Q is the flow rate of the solution (m^3/min), A is the area under graph $C(t)$ expressed in $\text{min} \cdot \text{mg}/\text{dm}^3$, and m is the mass of the bed (g), t_{total} is the total flow time (min).

The optimal values of sorption parameters were determined by the CCD (central composite design) analysis and the regression equation was obtained:

$$q_{eq} = a_0 + \sum_{i=1}^k a_i \cdot x_i + \sum_{i=1}^k a_{ii} \cdot x_i^2 + \sum_{i < j}^k a_{ij} \cdot x_i \cdot x_j \quad (8)$$

where x are independent variables and a_i, a_{ii}, a_{ij} are equation coefficients. The statistical analysis was carried out using STATISTICA (version 10.0).

Table 1. Experimental range and levels of independent process variables.

	Variable Name	Unit	Variable Symbol	Range	
				(−1)	(+1)
Ag ⁺	Height of adsorbent bed	(cm)	x_1	3	9
	Initial metal ion concentration	(mg dm ^{−1})	x_2	3000	5000
	Flow rate	(cm ³ min ^{−1})	x_3	2	4
Cu ²⁺	Height of adsorbent bed	(cm)	x_1	3	9
	Initial metal ion concentration	(mg dm ^{−1})	x_2	3000	5000
	Flow rate	(cm ³ min ^{−1})	x_3	3	6

2.5. Sorption Dynamics

The total capacity of vermiculite for a given initial concentration and flow rate is equal to the area under the plot of the adsorbed metal ion concentration versus effluent time. The capacity was evaluated from the experimental points of the curve, as shown in Equation (9):

$$q_{total} = \frac{Q \cdot A}{1000} = \frac{Q}{1000} \int_{t=0}^{t=t_{total}} C(t) dt = q_{eq} \cdot m \quad (9)$$

where t_{total} is the total flow time (min), Q is the flow rate (cm³/min) and A is the area under the breakthrough curve.

The total amount of Ag⁺ or Cu²⁺ theoretically adsorbed by the column is determined by the relation

$$M_{total} = \frac{C_0 \cdot Q \cdot t_{total}}{1000} \quad (10)$$

Knowing the total mass of adsorbed metal ions and the total sorbent capacity, it is possible to calculate the total percent of Ag⁺ and Cu²⁺ removed:

$$Y = \left(\frac{q_{total}}{M_{total}} \right) \cdot 100\% \quad (11)$$

In order to predict the dynamic behaviour of the column, many models (Clark, Bohart-Adams, Yoon-Nelson and Thomas) are used. It is important to predict the breakthrough curve for effluent parameters for the successful design of a column adsorption process.

2.6. Models

Breakthrough curves are used to describe the dynamics of the adsorption process. These are concentration plots which refer to the initial concentration depending on the process duration [19,20]. The appearance of the curves illustrates the course of the process, that is, the way in which the filling is saturated with the substance. The steeper the curve, the more effective the process. The course of the curve is predicted using adsorption dynamics models. These equations make it possible to determine the value of individual kinetic coefficients and the maximum adsorbent bed capacity of the adsorbent bed [21]. Most of these equations can be written in the general form as

$$\frac{C}{C_0} = [m + \exp(a + bt)]^n \quad (12)$$

where m , n , a and b are parameters that depend on the model.

Parameters assume different values due to different assumptions that simplify the model. Models that determine the dynamics of the adsorption process include the mass balance equations and process kinetics but skip the equation of heat balance (assuming that adsorption is carried out under isothermal conditions). Table 2 compares the adsorption dynamics models and the form of their nonlinear and linear equations.

2.6.1. The Bohart–Adams Model

Based on a theory of surface reactions, the Bohart–Adams model assumes that equilibrium is not instantaneous, and that the adsorption rate is proportional to the adsorption capacity of the sorbent [22]. The Bohart–Adams model describes the initial course of the breakthrough curve when the adsorbent still has the most active sites. The model is particularly useful for estimating characteristic parameters such as the maximum adsorption capacity and the kinetic constant used to determine a quasi-chemical kinetic rate expression [23].

2.6.2. The Thomas Model

The Thomas model is another that is frequently applied to estimate the adsorptive capacity of an adsorbent and predict breakthrough curves. The basic assumption of the Thomas model is that the process follows pseudo–second–order reversible reaction kinetics and the Langmuir isotherm for equilibrium. The model estimates the adsorption process where external and internal diffusion resistances may be negligible. The advantages of this model are its simplicity and reasonable accuracy in predicting the breakthrough curves under various operating conditions [24].

2.6.3. The Yoon–Nelson Model

The Yoon–Nelson equation has the simplest form of the applied models. This model does not include any process parameters. The advantage of the Yoon–Nelson model is its simpler form compared to the other models, and the lack of detailed data on the adsorbate and adsorbent character. The model is based on the assumption that the rate of decrease in the probability of adsorption for each adsorbate molecule is proportional to the probability of the adsorbate adsorption and the adsorbate breakthrough on the adsorbent [25,26].

2.6.4. The Clark Model

The Clark model is based on the assumption that the shape of the mass transfer zone is constant, and that all adsorbents are removed at the end of the column. Initially, this model was developed for the adsorption of organic compounds on activated carbon. However, the Clark model successfully works for other cases, including systems that have a variable mass transfer zone. The assumption of the Clark model is that the process follows the Freundlich isotherm for equilibrium [27,28].

Table 2. Models for fixed-bed column description.

Model	Nonlinear Form	Linear Form	Plot
Bohart-Adams	$\frac{C}{C_0} = \exp(k_{BA} \cdot C_0 \cdot t - k_{BAN_0} \cdot \frac{H}{u})$	$\ln \frac{C}{C_0} = k_{BA} \cdot C_0 \cdot t - k_{BA} \cdot q_{max} \cdot \frac{H}{u}$	$\frac{C}{C_0}$ vs t
Thomas	$\frac{C}{C_0} = \frac{1}{1 + e^{((\frac{k_{Th}}{Q}) \cdot q_{max} \cdot m - C_0 \cdot k_{Th} \cdot t)}}$	$\ln \left(\frac{C_0}{C} - 1 \right) = \left(\frac{k_{Th}}{Q} \right) \cdot q_{max} \cdot m - C_0 \cdot k_{Th} \cdot t$	$\frac{C}{C_0}$ vs t
Yoon-Nelson	$\frac{C}{C_0} = \frac{e^{k_{YN} \cdot (t-\tau)}}{1 + e^{k_{YN} \cdot (t-\tau)}}$	$\ln \frac{C}{C_0 - C} = k_{YN} \cdot t - k_{YN} \cdot \tau$	$\frac{C}{C_0}$ vs t
Clark	$\frac{C}{C_0} = \left(\frac{1}{1 + A_C \cdot e^{-r \cdot t}} \right)^{\frac{1}{n_F - 1}}$	$\ln \left[\left(\frac{C_0}{C} \right)^{n-1} - 1 \right] = -r \cdot t + \ln(A_C)$	$\frac{C}{C_0}$ vs t

3. Results and Discussion

3.1. Instrumental Analysis

The specific surface area and pore diameters of vermiculite were analyzed before and after the activation of NaOH and citric acid. Densitometric analysis makes it possible to establish the density of the material. The results for density (apparent, actual, bulk and relative) and porosity (total and open) are listed in Table 3. Figures 1 and 2 present sorption isotherms and the distribution of pore volume for raw and activated material. Vermiculite is a mesoporous material. Activated vermiculite compared to the raw material is characterized by a smaller specific surface area and a bigger share of mesopores (Figure 2). Basic or acid treatment caused leaching of octahedral layers and dissolution

of the amorphous phase leaving a material. Chemical activation decreased the layer charge of the material, facilitating ion exchange [29]. The smaller specific surface area is compensated by a high total porosity, which translates into its sorption capacity.

Table 3. Parameters of microstructural raw and activated vermiculite.

Variable	Raw Vermiculite	Base-Activated Vermiculite	Acid-Activated Vermiculite
Specific surface area (m^2/g)	29.93	2.152	2.777
Average pore diameter (nm)	0.558	1.487	1.737
Mesopore diameter (nm)	38.73	38.73	21.433
Bulk density d_b (g/cm^3)	0.2393 ± 0.0012	0.2460 ± 0.0018	0.2775 ± 0.0031
Apparent density d_p (g/cm^3)	1.4893 ± 0.0032	1.5550 ± 0.0929	1.6757 ± 0.1118
Actual density d_a (g/cm^3)	2.3427 ± 0.0060	2.4381 ± 0.0213	2.6923 ± 0.0443
Relative density (%)	10.21 ± 0.20	10.09 ± 0.08	10.31 ± 0.07
Total porosity (%)	89.79 ± 0.20	89.91 ± 0.08	89.69 ± 0.07
Open porosity (%)	83.93 ± 0.38	84.18 ± 0.02	83.44 ± 0.03

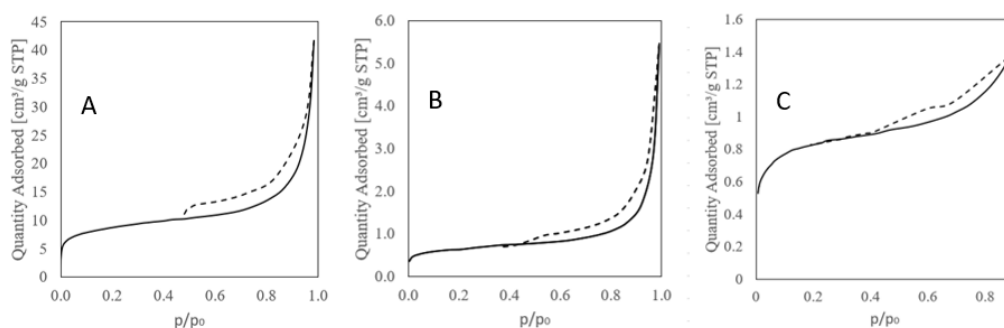


Figure 1. Sorption isotherms: (A) Raw vermiculite, (B) basic-activated vermiculite, (C) acid-activated vermiculite, (solid line-adsorption, dashed line-desorption).

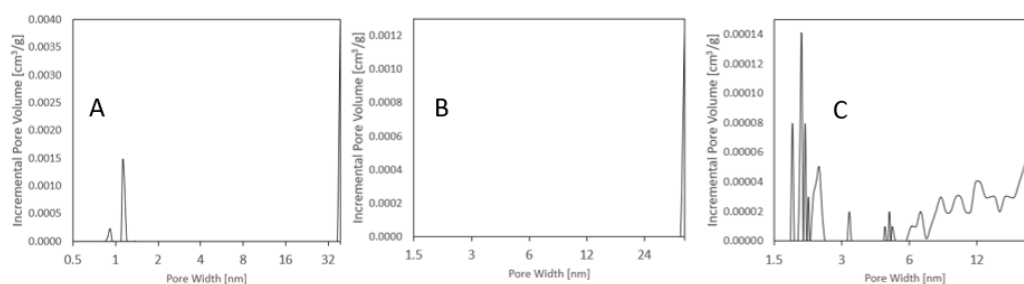


Figure 2. Distribution of pore volume relative to pore width: (A) Raw vermiculite, (B) basic-activated vermiculite, (C) acid-activated vermiculite.

Raw vermiculite, vermiculite modified with sodium hydroxide solution or citric acid solution, and vermiculite following the adsorption of metal ions, were subjected to XRD analysis (Figure 3). The analyzed samples were characterized by high purity. Stawiński et al. analyzed the structure of vermiculite and distinguished characteristic reflexes for it, including $5.6^\circ 2\theta$, $9.5^\circ 2\theta$, and $28.6^\circ 2\theta$. The results of analysis suggest damage to the crystalline structure of vermiculite as a result of the base and acid action. The results of chemical analysis confirm that components of the octahedral layer were dissolved under base action to a large extent. A decrease in the crystalline form of vermiculite was also confirmed by studies carried out on nitric and citric acid-modified vermiculite [29]. The changes in vermiculite structure were also confirmed by FTIR analysis (Figure 4). A broad peak between 900 and 1100 cm^{-1} confirms the presence of Si–O and Si–O–Si groups. Characteristic vermiculite bands are summarized in Table 4. The main change in structure of vermiculite is the presence of a nitro group ($-\text{O}_2$ stretching), which is confirmed by the presence of the peak at 1350 cm^{-1} (Figure 4D). The presence of nitro groups results from nitrate ions entering the AgNO_3 salt solution.

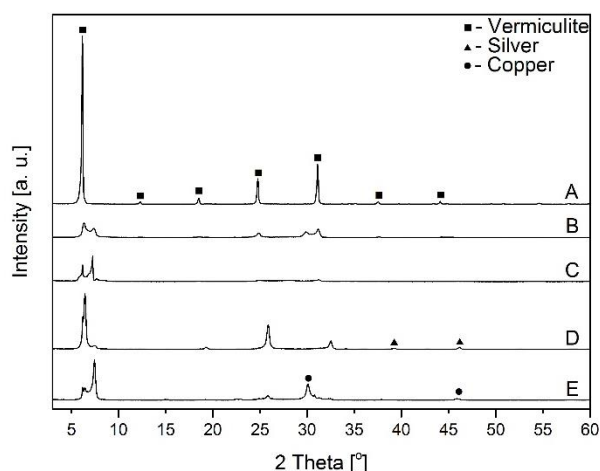


Figure 3. X-ray diffraction of vermiculite before and after Ag^+ or Cu^{2+} adsorption: A–raw vermiculite, B–NaOH-activated vermiculite, C–citric acid-activated vermiculite, D–vermiculite after the adsorption of silver ions, E–vermiculite after the adsorption of copper ions.

Table 4. FTIR characteristic peaks of vermiculite before and after Ag^+ / Cu^{2+} adsorption.

Vermiculite FTIR Peaks [cm^{-1}]	Assignment	References
440–450	Si–O–Si bending vibration	[30]
670–80	Si–O–Si asymmetric stretching	[31]
730–760	Al–O coordination	[32]
1000–1010	Si–O asymmetric stretching	[33]
1100–1125	Si–O–Si asymmetric stretching	[30]
1350	N=O stretching	[32]
1630–1650	O–H bending mode	[34]
3350–3450	O–H stretching	[35]

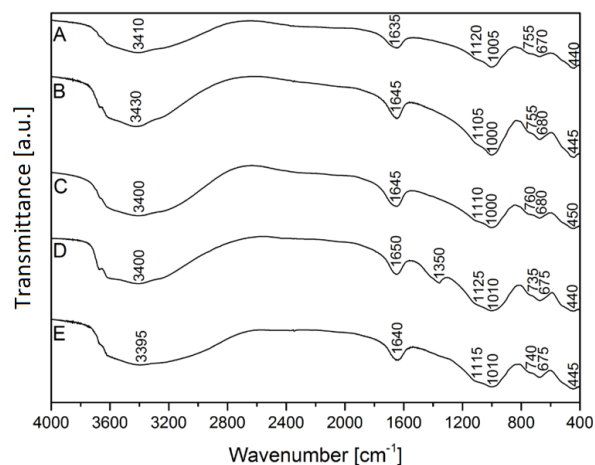


Figure 4. FTIR analysis of vermiculite: A–raw vermiculite, B–NaOH-activated vermiculite, C–citric acid-activated vermiculite, D–vermiculite after the adsorption of silver ions, E–vermiculite after the adsorption of copper ions.

Figure 5 shows the SEM micrographs of vermiculite before and after Ag^+ and Cu^{2+} adsorption. The microphotographs analysis revealed a plate structure of vermiculite [36,37]. The EDS technique revealed the presence of a number of elements. The base-activated material additionally contains sodium, which suggests the replacement of Mg^{2+} with Na^+ [36]. After adsorption of silver ions, the material additionally contained silver or copper. The presence of both elements on the surface of vermiculite confirmed the effectiveness of the adsorption process. Table 5 presents a comparison

of the maximum sorption capacities for metal ions of the raw and modified vermiculite found in the literature. Modified vermiculite is characterized by a higher sorption capacity compared to the raw material, which confirms a beneficial effect of activation processes on vermiculite.

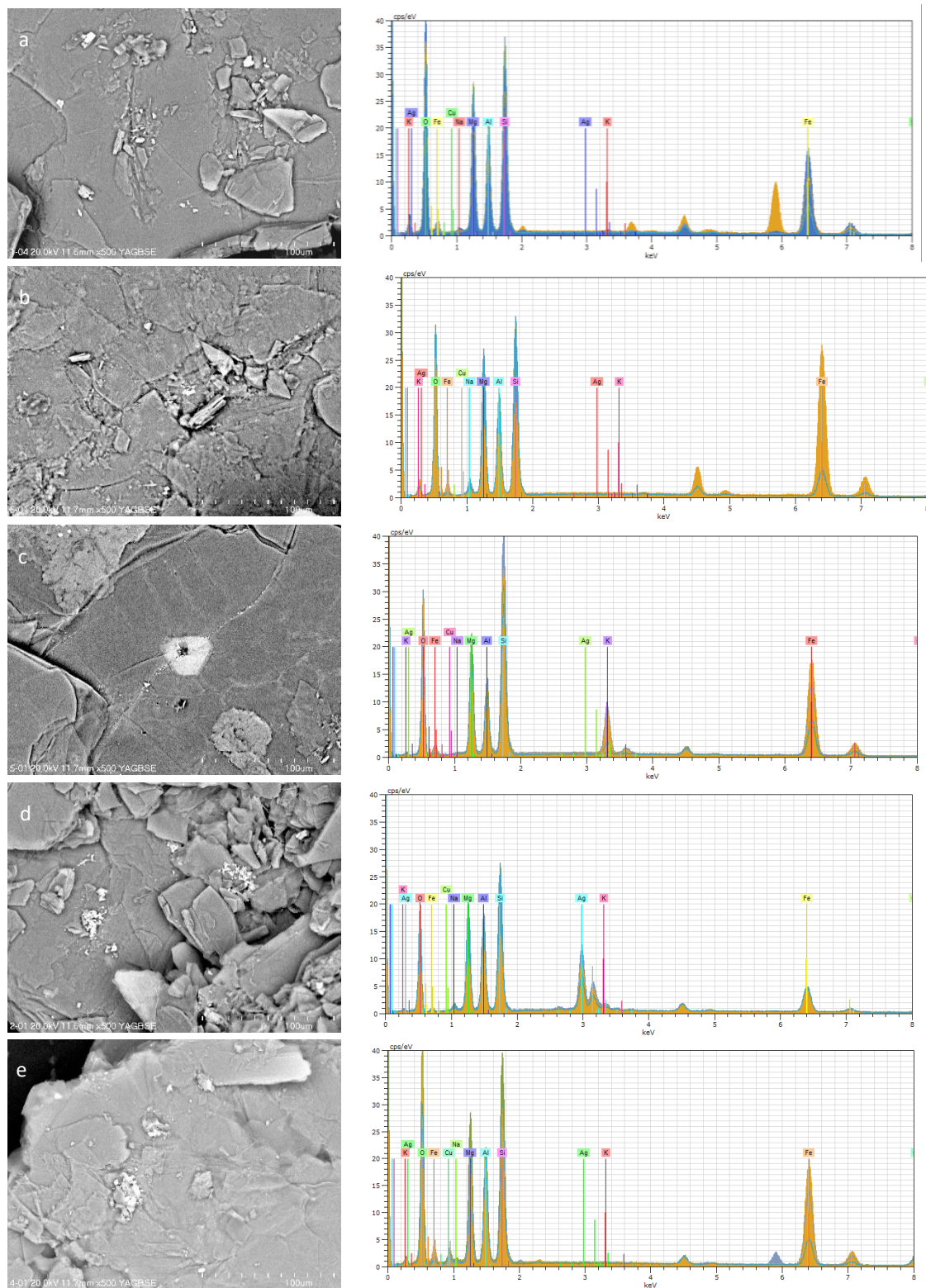


Figure 5. SEM images and EDS patterns of vermiculite: (a) Raw vermiculite, (b) NaOH-activated vermiculite, (c) citric acid-activated vermiculite, (d) after the adsorption of Ag^+ , (e) after the adsorption of Cu^{2+} .

Table 5. Comparison of sorption capacities of vermiculite for several sorbents.

Sorbent	$q_{(Cu^{2+})}$ (mg/g)	$q_{(Ag^+)}$ (mg/g)	$q_{(As^{3+})}$ (mg/g)	$q_{(Ni^{2+})}$ (mg/g)	$q_{(Zn^{2+})}$ (mg/g)	$q_{(Pb^{2+})}$ (mg/g)	Ref.
Raw vermiculite	20.61	46.9	34.9	25.33	23.40	64.10	[15,38]
Alkaline treated vermiculite	51.1	71.2	–	–	–	–	[18,29]
Chitosan-modified vermiculite	–	–	72.2	–	–	–	[16]
Vermiculite (adsorption in multi-component systems)	–	2.7–12.2	–	8.1–14.2	–	20–68	[39]

3.2. The Best Values of Parameters

Table 6 presents the total bed capacity and the total percentage of Ag^+ and Cu^{2+} removed under different conditions. The maximum sorption capacity increases with the initial concentration of metal ions and decreases with the bed height and flow rate. The maximum total percentage of metal ions amounted to 60.4% and 68.7% for Ag^+ and Cu^{2+} , respectively.

Table 6. Column data parameters obtained at different inlet metal ion concentrations, bed heights and flow rates.

Run	Ag^+					Cu^{2+}				
	C_0 ($\frac{mg}{dm^3}$)	h (cm)	Q ($\frac{cm^3}{min}$)	q_{eq} (mg/g)	Y (%)	C_0 ($\frac{mg}{dm^3}$)	h (cm)	Q ($\frac{cm^3}{min}$)	q_{eq} (mg/g)	Y (%)
1	3000	3	2	29.70	52.66	3000	3	3	41.45	59.56
2	3000	3	4	23.96	44.38	3000	3	6	28.39	65.62
3	3000	9	2	8.89	17.41	3000	9	3	19.70	58.62
4	3000	9	4	19.06	44.95	3000	9	6	19.80	49.50
5	5000	3	2	68.89	60.43	5000	3	3	59.10	68.76
6	5000	3	4	61.96	59.37	5000	3	6	26.02	40.66
7	5000	9	2	29.20	53.11	5000	9	3	48.85	56.08
8	5000	9	4	19.42	45.29	5000	9	6	38.20	58.47
9	3000	6	3	17.46	37.86	3000	6	4.5	14.58	52.81
10	5000	6	3	40.93	58.71	5000	6	4.5	43.05	67.16
11	4000	3	3	30.55	48.96	4000	3	4.5	55.21	66.00
12	4000	9	3	29.24	46.87	4000	9	4.5	46.90	62.81
13	4000	6	2	11.87	23.56	4000	6	3	33.58	46.64
14	4000	6	4	22.75	49.03	4000	6	6	27.02	58.23
15	4000	6	3	23.17	59.30	4000	6	4.5	33.10	60.85
16	4000	6	3	21.50	52.09	4000	6	4.5	31.98	60.57
17	4000	6	3	18.23	41.07	4000	6	4.5	36.66	67.40
18	4000	6	3	20.94	45.94	4000	6	4.5	35.52	63.42
19	4000	6	3	25.27	46.80	4000	6	4.5	29.85	56.52

Figure 6 shows Pareto charts of standardized results. At an assumed significance level of 5.0%, all parameters in the case of silver ion sorption have a significant influence on the adsorption process, while in the case of copper ion adsorption, the initial concentration of the metal ion solution and the adsorbent height have a significant influence.

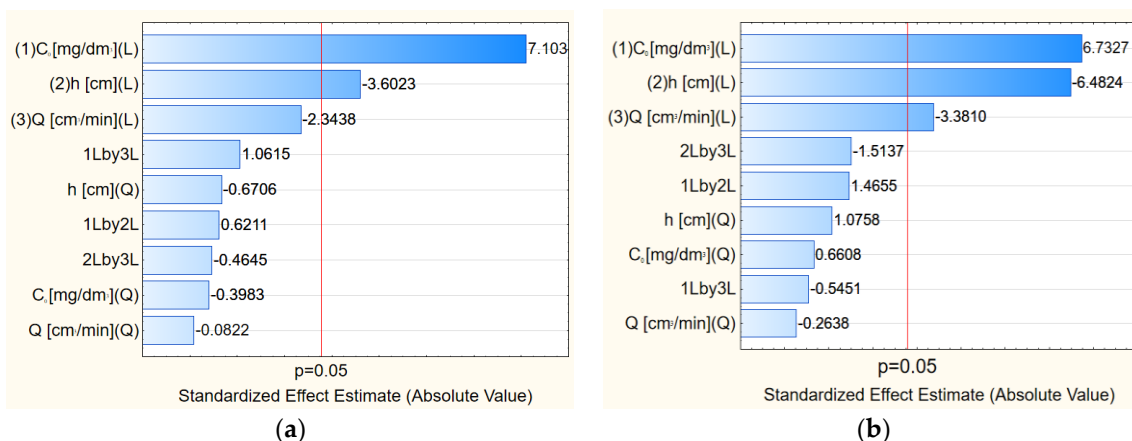


Figure 6. Pareto chart of standardized experimental effects for vermiculite: (a) For silver ions and (b) for copper ions.

The profile for predicted values and desirability options in the STATISTICA software is used for the optimization process. The CCD optimization design matrix (Figure 7) shows the maximum removal (60.43 and 68.76% for Ag⁺ and Cu²⁺, respectively) under the following conditions: 3 cm bed height, 5000 mg/cm³ initial metal ions concentration, and 2 cm³/min and 3 cm³/min flow rate for Ag⁺ and Cu²⁺, respectively.

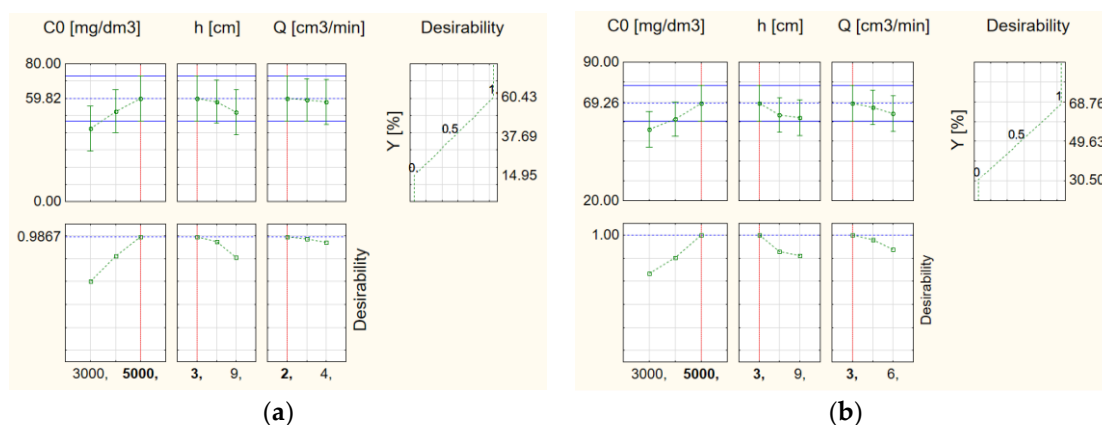


Figure 7. Profiles for predicted values and desirability for the removal of: (a) silver ions, (b) copper ions

3.2.1. Influence of Initial Concentration

A study was carried out to determine the influence of the concentration of the feed solution on the adsorption of silver and copper ions in the fixed-bed column within the range of 3000–5000 mg/dm³. Figure 8 shows the breakthrough curves for three different initial concentrations of metal cations. As expected, the initial concentration affects the breakthrough curves to a great extent. The highest sorption capacity was achieved at the highest concentration of feed solution. On the other hand, the greater the concentration, the lower the degree of adsorption. The initial slope of the breakthrough curves became more precipitous when the initial concentration was increased, showing that the reaction zone advances faster under high load conditions. In contact with a more concentrated metal ion solution, the bed is more saturated, which influences the concentration gradient (ΔC) that drives the process. The higher the ΔC , the faster the process. At lower concentrations, the process is characterized by a lower value of ΔC , which results in a slower rate but a higher degree of adsorption. Yahaya et al. investigated the effect of inlet initial Cu²⁺ concentration for a bed height of 60 mm and a solution flow rate of 10 cm³/min [23]. This confirmed the fact that the larger the inlet concentration, the steeper the slope of the breakthrough curve.

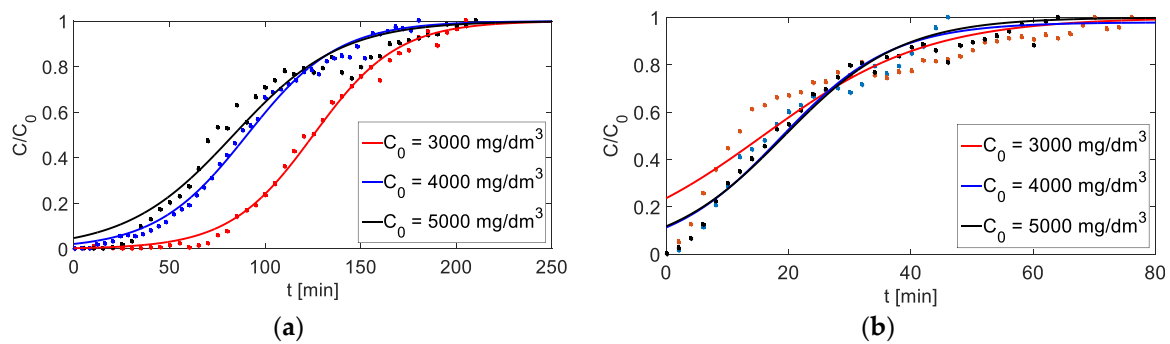


Figure 8. Breakthrough curves for different initial concentrations of metal cations: (a) Ag^+ adsorption ($h = 6$ cm, $Q = 3$ cm³/min), (b) Cu^{2+} adsorption ($h = 6$ cm, $Q = 4.5$ cm³/min).

3.2.2. Influence of Bed Height

The breakthrough curve was examined for the adsorption of Ag^+ and Cu^{2+} solutions for the effect of bed height. In order to perform this study, breakthrough curves at different bed heights (3, 6 and 9 cm) and with the same influent concentration ($C_0 = 4000$ mg/dm³) and flow rate ($Q = 3.0$ or $Q = 4.5$ cm³/min, for silver and copper respectively), were plotted. Figure 9 shows that as the bed height increases, the breakthrough curve is gentler and flattened. When the bed height increased, metal cations had more time for contact with vermiculite, which resulted in the increased removal of silver and copper ions. At larger bed heights, some of the active sites will be bypassed by metal ions, hence the total efficiency of the deposit will decrease. The slope of the breakthrough curve increased with a decreasing bed height, which resulted in a reduced mass transfer zone, and the proportion of adsorbent replete with metal ions increased.

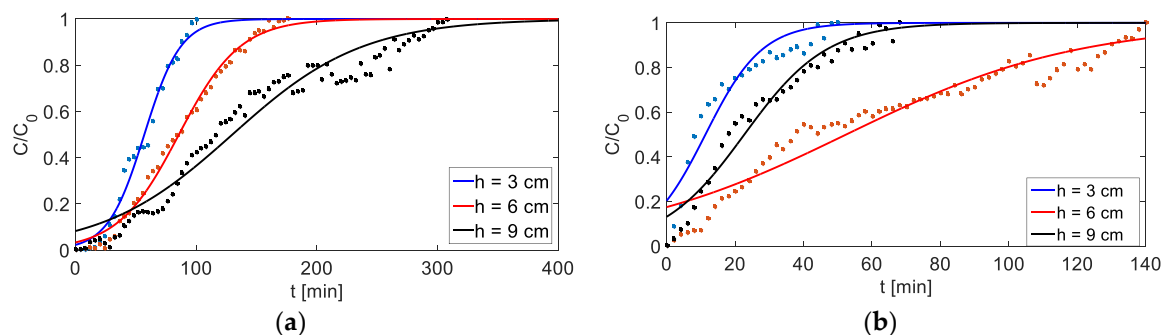


Figure 9. Breakthrough curves for different bed heights: (a) Ag^+ adsorption ($C_0 = 4000$ mg/dm³, $Q = 3$ cm³/min), (b) Cu^{2+} adsorption ($C_0 = 4000$ mg/dm³, $Q = 4.5$ cm³/min).

3.2.3. Influence of Flow Rate

Changing the flow rate has the slightest effect on the sorption process of silver and copper ions. The effect of feed flow rate was investigated by changing the feed flow rate from 2 and 3 to 4 and 6 cm³/min for silver and copper ions, respectively. The breakthrough curves at a constant bed height and constant initial concentration of metal cations are shown in Figure 10. The slope of the breakthrough curves increases as the flow rate increases. Mukhopadhyay et al. conducted the biosorption of copper(II) ions. They noted that the flow rate had a significant influence on the course of the breakthrough curve [34]. Analyzing the effect of the flow rate on Ag^+ and Cu^{2+} adsorption showed that full bed saturation was faster at higher flow rates of solutions. It follows that the degree of adsorption decreases as the flow rate of the adsorbate solution increases. At a low rate of influent, metal cations had more time for contact with vermiculite, which resulted in the increased removal of silver and copper ions from the column, and the efficiency of the sorption process improved. Furthermore, the lower the flow of the feed solution, the less wastewater is produced.

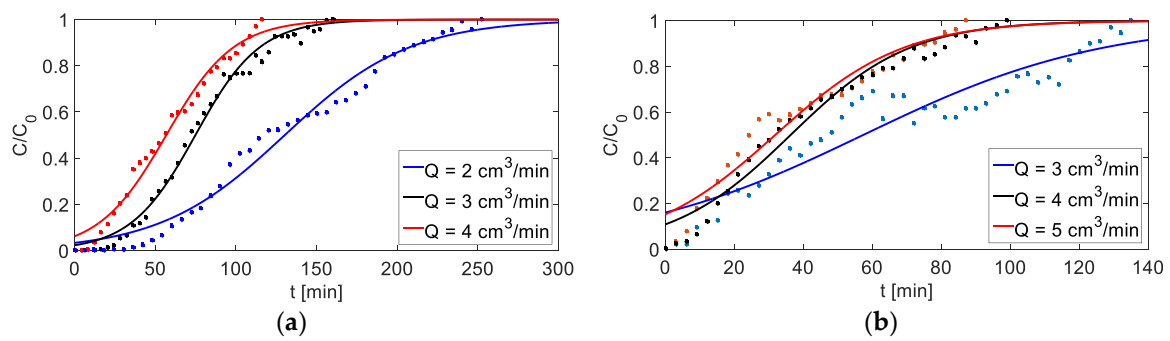


Figure 10. Breakthrough curves for different flow rates of feed solution ($C_0 = 4000 \text{ mg/dm}^3$, $h = 6 \text{ cm}$): (a) Ag^+ adsorption, (b) Cu^{2+} adsorption.

3.3. Dynamics Studies

Dynamic analysis was performed for measurements with optimal process parameters, that is, a bed height of 3 cm, flow rate for adsorption of Ag^+ at $2 \text{ cm}^3/\text{min}$ or for adsorption of Cu^{2+} at $3 \text{ cm}^3/\text{min}$, and initial concentrations of silver or copper ion solutions of 5000 mg/dm^3 . For kinetic analysis of the adsorption process in the column, four kinetic models were used: Bohart-Adams, Thomas, Yoon-Nelson and Clark. Table 7 presents values of the coefficients of equations and the degree of correspondence between the theoretical approximation and the experimental data. Figure 11 shows the course of curves and experimental points with the nonlinear regression of models. The Clark model gave the best predictions of experimental behaviour for the adsorption of both silver and copper ions. Apparently, only slight differences from the other models were observed and the compatibility of models with experimental parameters was similar. On this basis, by analyzing only model parameters, it is difficult to obtain relevant information from the adsorption mechanism and the nature of the process. To choose or develop a suitable model, accuracy and convenience should be considered simultaneously. The dynamics of copper ion adsorption in a fixed-bed column system were investigated by Yahaya et al. According to Yahaya et al., the column experimental data were well-fitted with both the Thomas and the Yoon-Nelson models, which also suggested slight differences in models results [25]. The experimental research confirmed that the Bohart–Adams, Thomas, and Yoon and Nelson models were equivalent mathematically: the breakthrough curves that describe the experimental points overlap [40].

Table 7. The Bohart–Adams, Thomas, Yoon–Nelson and Clark model parameters using nonlinear regression analysis.

Isotherm	Parameters	Adsorbed Metal Ions	
		Ag^+	Cu^{2+}
Bohart–Adams	$k_{\text{BA}} \left(\text{dm}^3 \text{min}^{-1} \text{mg}^{-1} \right)$	0.0071 ± 0.0003	0.021 ± 0.004
	$N_0 \left(\text{mg l}^{-1} \right)$	0.51 ± 0.005	0.50 ± 0.04
	R^2_{adjusted}	0.9729	0.9548
	F	649.8	277.2
Clark	A_c	2.7 ± 0.3	2.3 ± 0.5
	$r \left(\text{min}^{-1} \right)$	0.015 ± 0.001	0.12 ± 0.0009
	R^2_{adjusted}	0.9943	0.9766
	F	531.1	121.7

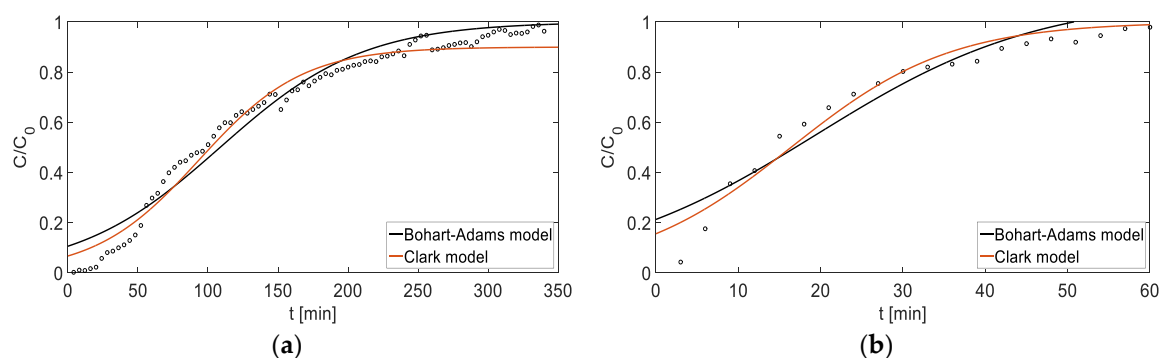


Figure 11. Fit of breakthrough curves with mathematical models: (a) Ag^+ adsorption ($C_0 = 5000 \text{ mg/dm}^3$, $h = 3 \text{ cm}$, $Q = 2 \text{ cm}^3/\text{min}$), (b) Cu^{2+} adsorption ($C_0 = 5000 \text{ mg/dm}^3$, $h = 3 \text{ cm}$, $Q = 3 \text{ cm}^3/\text{min}$).

4. Conclusions

This study has shown that vermiculite may be successfully used as an inexpensive sorbent in the process of adsorption of silver and copper ions in aqueous solution in a column system. The experiments allowed us to determine that optimal conditions for the process of sorption of silver and copper ions include an initial concentration of metal ion solution of 5000 mg/dm^3 , a flow rate of $2 \text{ cm}^3/\text{min}$ and $3 \text{ cm}^3/\text{min}$ for silver and copper ions, respectively, and a bed height of 3 cm . The degree of adsorption was 60% and 69% for Ag^+ and Cu^{2+} , respectively. The initial silver and copper ion concentration changes were most influenced by the adsorption process. The column data were best-fitted with the Clark model and could be used to determine the characteristic parameters of the column used for the process. From the analysis of the influence of factors, it follows that the greater the adsorption capacity of vermiculite, the steeper the breakthrough curves. A lower bed height, a larger initial metal cation concentration and a lower solution flow rate all improve the efficiency of the sorption capacity of vermiculite.

Author Contributions: conceptualization, M.B.; methodology, M.B. and O.D.; formal analysis, O.D.; investigation, O.D.; resources, O.D.; data curation, M.B. and O.D.; writing—original draft preparation, O.D.; writing—review and editing, M.B.; visualization, O.D.; supervision, M.B.

Funding: This research did not receive any specific grant from funding agencies in the public, commercial, or not-for-profit sectors.

Conflicts of Interest: The authors report no declarations of conflict of interest.

References

1. Kyzas, G.Z.; Kostoglou, M. Green Adsorbents Wastewaters: A Critical Review. *Materials* **2014**, *7*, 333–364. [[CrossRef](#)] [[PubMed](#)]
2. Inglezakis, V.J.; Elaiopoulos, K.; Aggelatou, V.; Zorpas, A.A. Treatment of underground water in open flow and closed-loop fixed bed systems by utilizing the natural minerals clinoptilolite and vermiculite. *Desalin. Water Treat.* **2012**, *39*, 215–227. [[CrossRef](#)]
3. Stylianou, M.A.; Inglezakis, A.J.; Moustakas, K.G.; Malamis, S.P.; Loizidou, M.D. Removal of Cu(II) in fixed bed and batch reactors using natural zeolite and exfoliated vermiculite as adsorbents. *Desalination* **2007**, *215*, 133–142. [[CrossRef](#)]
4. Fernando, S.; Gunasekara, T.; Holton, J. Antimicrobial Nanoparticles: Applications and mechanisms of action. *Sri Lankan J. Infect. Dis.* **2018**, *2*, 2–11. [[CrossRef](#)]
5. Xiu, Z.-M.; Ma, J.; Alvarez, P.J.J. Differential Effect of Common Ligands and Molecular Oxygen on Antimicrobial Activity of Silver Nanoparticles versus Silver Ions. *Environ. Sci. Technol.* **2011**, *45*, 9003–9008. [[CrossRef](#)] [[PubMed](#)]
6. Mishra, S.P. Adsorption–desorption of heavy metal ions. *Curr. Sci.* **2014**, *107*, 601–612.

7. Rogala, Z. Adsorption chiller using flat-tube adsorbers—Performance assessment and optimization. *Appl. Therm. Eng.* **2017**, *121*, 431–442. [[CrossRef](#)]
8. Hasany, S.M.; Saeed, M.M.; Ahmed, M. Sorption of traces of silver ions onto polyurethane foam from acidic solution. *Talanta* **2001**, *54*, 89–98. [[CrossRef](#)]
9. Abollino, O.; Giacomino, A.; Malandrino, M.; Mentasti, E. Interaction of metal ions with montmorillonite and vermiculite. *Appl. Clay Sci.* **2008**, *38*, 227–236. [[CrossRef](#)]
10. Tan, K.L.; Hameed, B.H. Insight into the adsorption kinetics models for the removal of contaminants from aqueous solutions. *J. Taiwan Inst. Chem. Eng.* **2017**, *74*, 25–48. [[CrossRef](#)]
11. Inglezakis, V.J.; Stylianou, M.; Loizidou, M. Ion exchange and adsorption equilibrium studies on clinoptilolite, bentonite and vermiculite. *J. Phys. Chem. Solids* **2010**, *71*, 279–284. [[CrossRef](#)]
12. Hashem, F.S.; Amin, M.S.; El-Gamal, S.M.A. Chemical activation of vermiculite to produce highly efficient material for Pb²⁺ and Cd²⁺ removal. *Appl. Clay Sci.* **2015**, *115*, 189–200. [[CrossRef](#)]
13. Rashad, A.M. Vermiculite as a construction material—A short guide for Civil Engineer. *Constr. Build. Mater.* **2016**, *125*, 53–62. [[CrossRef](#)]
14. Badawy, N.A.; El-Bayaa, A.A.; Abd AlKhalik, E. Vermiculite as an exchanger for copper(II) and Cr(III) ions, kinetic studies. *Ionics* **2010**, *16*, 733–739. [[CrossRef](#)]
15. Malandrino, M.; Abollino, O.; Giacomino, A.; Aceto, M.; Mentasti, E. Adsorption of heavy metals on vermiculite: Influence of pH and organic ligands. *J. Colloid Interface Sci.* **2006**, *299*, 537–546. [[CrossRef](#)] [[PubMed](#)]
16. Saleh, A.T.; Sari, A.; Tuzen, M. Chitosan-modified vermiculite for As(III) adsorption from aqueous solution: Equilibrium, thermodynamic and kinetic studies. *J. Mol. Liq.* **2016**, *219*, 937–945. [[CrossRef](#)]
17. Narasimha, K.N.P.; Ramalingaiah, H.; Melka, K.; Krishnaveni, K.; Prasad, P.S.R.; Krishnaiah, C.; Jayappa, K.S.; Ganesha, A.V. Vermiculite mineralization associated with ultramafics in Agasthyapura Area, Mysore Dist., Karnataka State, India—A Mineralogical Study. *Acta Geodyn. Geomater.* **2006**, *3*, 19–31.
18. Długosz, O.; Banach, M. Kinetic, isotherm and thermodynamic investigations of the adsorption of Ag⁺ and Cu²⁺ on vermiculite. *J. Mol. Liq.* **2018**, *258*, 295–309. [[CrossRef](#)]
19. Xavier, A.L.P.; Adarme, O.F.H.; Furtado, L.M.; Ferreira, G.M.D.; Mendes da Silva, L.H.; Gil, L.F.; Gurgel, L.V.A. Modeling adsorption of copper(II), cobalt(II) and nickel(II) metal ions from aqueous solution onto a new carboxylated sugarcane bagasse. Part II: Optimization of monocomponent fixed-bed column adsorption. *J. Colloid Interface Sci.* **2018**, *516*, 431–445. [[CrossRef](#)] [[PubMed](#)]
20. Ruiz, M.; Roset, L.; Demey, H.; Castro, S.; Sastre, A.M.; Perez, J.J. Equilibrium and dynamic studies for adsorption of boron on calcium alginate gel beads using principal component analysis (PCA) and partial least squares (PLS). *Mater. Sci. Eng. Technol.* **2013**, *44*, 410–415. [[CrossRef](#)]
21. Ahmed, A.A.; Idris, A.; Hameed, B.H. Modeling of disperse dye adsorption onto bamboo-based activated carbon in fixed-bed column. *Desalin. Water Treat.* **2014**, *52*, 248–256. [[CrossRef](#)]
22. Bohart, G.S.; Adams, E.Q. Some aspects of the behavior of the charcoal with respect chlorine. *J. Am. Chem. Soc.* **1920**, *42*, 523–544. [[CrossRef](#)]
23. Inglezakis, V.J. Ion exchange and adsorption fixed bed operations for wastewater treatment—Part I: Modeling fundamentals and hydraulics analysis. *J. Eng. Stud. Res.* **2010**, *16*, 29–41.
24. Dantas, T.L.P.; Luna, F.M.T.; Silve, I.J., Jr.; Torres, A.E.B.; de Azevedo, D.C.S.; Rodrigues, A.E.; Moreira, R.F.P.M. Modeling of the fixed-bed adsorption of carbon dioxide and a carbon dioxide nitrogen mixture on zeolite 13x. *Braz. J. Chem. Eng.* **2011**, *28*, 533–544. [[CrossRef](#)]
25. Yahaya, N.K.; Abustan, I.; Latiff, M.F.P.M. Fixed-bed Column Study for Cu (II) Removal from Aqueous Solutions using Rice Husk based Activated Carbon. *Int. J. Eng. Technol.* **2011**, *11*, 186–190.
26. Yoon, Y.H.; Nelson, J.H. Application of gas adsorption kinetics. Part 1. A theoretical model for respirator cartridge service time. *Am. Ind. Hyg. Assoc. J.* **1984**, *45*, 509–516. [[CrossRef](#)] [[PubMed](#)]
27. Xu, Z.; Cai, J.; Pan, B. Mathematically modeling fixed-bed adsorption in aqueous systems. *Appl. Phys. Eng.* **2013**, *14*, 155–176. [[CrossRef](#)]
28. Clark, R.M. Modeling TOC removal by GAC: The general logistic function. *J. Am. Water Works Assoc.* **1987**, *79*, 33–131. [[CrossRef](#)]
29. Stawiński, W.; Węgrzyn, A.; Dańko, T.; Freitas, O.; Figueiredo, S.; Chmielarz, L. Acid-base treated vermiculite as high performance adsorbent: Insights into the mechanism of cationic dyes adsorption, regeneration, recyclability and stability studies. *Chemosphere* **2017**, *173*, 107–115. [[CrossRef](#)] [[PubMed](#)]

30. Sutcu, M. Influence of expanded vermiculite on physical properties and thermal conductivity of clay bricks. *Ceram. Int.* **2015**, *41*, 2819–2827. [[CrossRef](#)]
31. Wang, M.; Liao, L.; Zhang, X.; Li, Z.; Xia, Z.; Cao, W. Adsorption of low-concentration ammonium onto vermiculite from Hebei Province, China. *Clays Clay Miner.* **2011**, *59*, 459–465. [[CrossRef](#)]
32. Lin-Vien, D.; Colthup, N.B.; Grasselli, J.H. *The Handbook of Infrared and Raman Characteristic Frequencies of Organic Molecules*; Academic Press: Cambridge, MA, USA, 1991.
33. Long, H.; Wu, P.; Yang, L.; Huang, Z.; Zhu, N.; Hu, Z. Efficient removal of cesium from aqueous solution with vermiculite of enhanced adsorption property through surface modification by ethylamine. *J. Colloid Interface Sci.* **2014**, *428*, 295–301. [[CrossRef](#)] [[PubMed](#)]
34. Mukhopadhyay, M.; Noronha, S.B.; Suraishkumar, G.K. Copper biosorption in a column of pretreated *Aspergillus niger* biomass. *Chem. Eng. J.* **2008**, *144*, 386–390. [[CrossRef](#)]
35. Huo, X.; Wu, L.; Liao, L.; Xia, Z.; Wang, L. The effect of interlayer cations on the expansion of vermiculite. *Powder Technol.* **2012**, *224*, 241–246. [[CrossRef](#)]
36. Santos, S.S.G.; Silva, H.R.M.; de Souza, A.G.; Alves, A.P.M.; da Silva Filho, E.C.; Fonseca, M.G. Acid-leached mixed vermiculites obtained by treatment with nitric acid. *Appl. Clay Sci.* **2015**, *104*, 286–294. [[CrossRef](#)]
37. Bindi, L.; Yao, N.; Lin, C.; Hollister, L.S.; Andronicos, C.L.; Distler, V.V.; Eddy, M.P.; Kostin, A.; Kryachko, V.; MacPherson, G.J.; et al. Natural quasicrystal with decagonal symmetry. *Sci. Rep.* **2015**, *5*, 1–5. [[CrossRef](#)] [[PubMed](#)]
38. El-Bayaa, A.A.; Badawy, N.A.; Abd, A.E. Effect of ionic strength on the adsorption of copper and chromium ions by vermiculite pure clay mineral. *J. Hazard. Mater.* **2009**, *170*, 1204–1209. [[CrossRef](#)] [[PubMed](#)]
39. Yong, L.; Hui, L.; Zhu, X.H. Competitive Adsorption of Ag^+ , Pb^{2+} , Ni^{2+} , and Cd^{2+} Ions on Vermiculite. *Sep. Sci. Technol.* **2010**, *45*, 277–287. [[CrossRef](#)]
40. Chu, K.H. Fixed bed sorption: Setting the record straight on the Bohart–Adams and Thomas models. *J. Hazard. Mater.* **2010**, *177*, 1006–1012. [[CrossRef](#)] [[PubMed](#)]



© 2018 by the authors. Licensee MDPI, Basel, Switzerland. This article is an open access article distributed under the terms and conditions of the Creative Commons Attribution (CC BY) license (<http://creativecommons.org/licenses/by/4.0/>).